Geopositioning Accuracy Assessment of GeoEye-1 Panchromatic and Multispectral Imagery

Manuel A. Aguilar, Fernando J. Aguilar, María del Mar Saldaña, and Ismael Fernández

Abstract

Currently GeoEye-1 is the World's highest resolution commercial satellite. This paper analyses the attainable geopositioning accuracy from a single GeoEye-1 Geo image, both through the sensor orientation and orthorectification phases, for panchromatic (PAN) and multispectral (MS) products.

Different 3D sensor models as well as the number and distribution of the ground control points (GCPs) used for the sensor orientation were tested. Planimetric Root Mean Square Errors ($RMSE_{2D}$) close to 0.7 pixels, both for PAN and MS images, were attained using the third order 3D rational functions with the vendor's rational polynomial coefficients data afterwards being refined by a zero order polynomial adjustment (RPC0). Furthermore, the RPC0 sensor model proved to be significantly independent regarding the number and distribution of the GCPs. The RPC0 model yielded $RMSE_{2D}$ close to 0.46 m and 1.56 m for the PAN and MS orthorectified images, respectively, using a very accurate lidar-derived digital elevation model.

Introduction

With the successful launch of the first very high resolution (VHR) satellites capable of capturing panchromatic (PAN) imagery of the land surface with Ground Sample Distance (GSD) even lower than 1 m, such as Ikonos in September 1999, and QuickBird in October 2001, many researchers have considered them as possible substitutes of conventional aerial photogrammetric mapping at large scales (e.g., Kay *et al.*, 2003; Aguilar *et al.*, 2007a; Li *et al.* 2007; Aguilar *et al.*, 2008a). Furthermore, during 2006 and 2007 many new commercially available VHR satellites, such as EROS B1, Resurs DK-1, KOMPSAT-2, IRS Cartosat 2, and WorldView-1, have been successfully launched, and they are offering to their customers both very high resolution imagery of the Earth and a very short revisit time.

More recently, a new VHR satellite named GeoEye-1 (GeoEye, Inc.) was launched in September 2008. Currently, it is the commercial satellite with the highest geometric resolution, 0.41 m GSD at nadir for PAN imagery and 1.65 m GSD at nadir for multispectral (MS), including the four classic bands (i.e., Red, Green, Blue, and Near Infrared). However, image products from GeoEye-1 have to be down-sampled to 0.5 m and 2 m GSD, PAN, and MS, respectively, for commercial sales, as a requirement levied by the US Government. Certainly, GeoEye-1, together with the last DigitalGlobe WorldView-2 satellite, the first VHR commercially available 8-band MS satellite launched in October 2009, are the two commercial VHR satellites more innovative and unexplored. In this way, the first geopositioning accuracy results attained in the orientation stage from GeoEye-1 PAN stereopairs were superior enough to those obtained from older satellites such as Ikonos or QuickBird. Fraser and Ravanbakhsh (2009) achieved vertical and horizontal accuracies of 0.25 m and 0.10 m, respectively, using a stereopair of GeoEye-1, whereas Mitchell and MacNabb (2010), working again onto a GeoEye-1 stereopair, reported a vertical Root Mean Square Error ($RMSE_z$) of 0.25 m by using a lidar-derived digital elevation model (DEM) comprising an area close to 50 km^2 as ground truth. Bearing in mind that these works were carried out in very well-controlled metric evaluation tests involving both highly accurate ground control points (GCPs) and independent checkpoints (ICPs) both in image and object spaces; it would be necessary to carry out more research under real operational conditions. In fact, a few more modest results close to 0.38 m planimetric accuracy and 0.7 m vertical accuracy were achieved by Meguro and Fraser (2010) from a GeoEye-1 stereopair. In this case, this accuracy loss could be explained by the use of natural features and unsignalized ground points which notably increased the image space pointing error of the GCPs and ICPs.

This work is part of a bigger program of research projects which are focused on the monitoring and modeling of the evolution and vulnerability of a pilot area, located at a coastal fringe of Almería (southeast of Spain), by means of multi-source and multi-temporal geospatial data. Furthermore, recently launched fine spatial resolution satellite sensing systems could be useful for detailed shoreline mapping and monitoring coastal applications (e.g., Muslim and Foody, 2008; Liu *et al.*, 2009). In this sense, the geometric accuracy capabilities of the newest VHR satellite images should be known.

Thus, the main objective of this paper was to perform a statistical analysis to determine the influence of several factors on the geopositioning accuracy capabilities of GeoEye-1 PAN and MS Geo singles images for producing orthorectified imagery under typical operational conditions. In this sense, the following variation sources have been studied: (a) different sensor orientation models have been tested to georeference the satellite data, (b) the number of GCPs, ranging from 2 up to 12, used in the orientation process, (c) distribution of GCPs, and finally (d) the vertical accuracy of the DEM employed in the orthorectification process.

Department of Agricultural Engineering. Almería University - Spain, Ctra. de Sacramento s/n, La Cañada de San Urbano, Escuela Superior de Ingeniería. 04120, Almería, Spain (maguilar@ual.es).

Photogrammetric Engineering & Remote Sensing
Vol. 78, No. 3, March 2012, pp. 247–257.

0099-1112/12/7803–247/$3.00/0

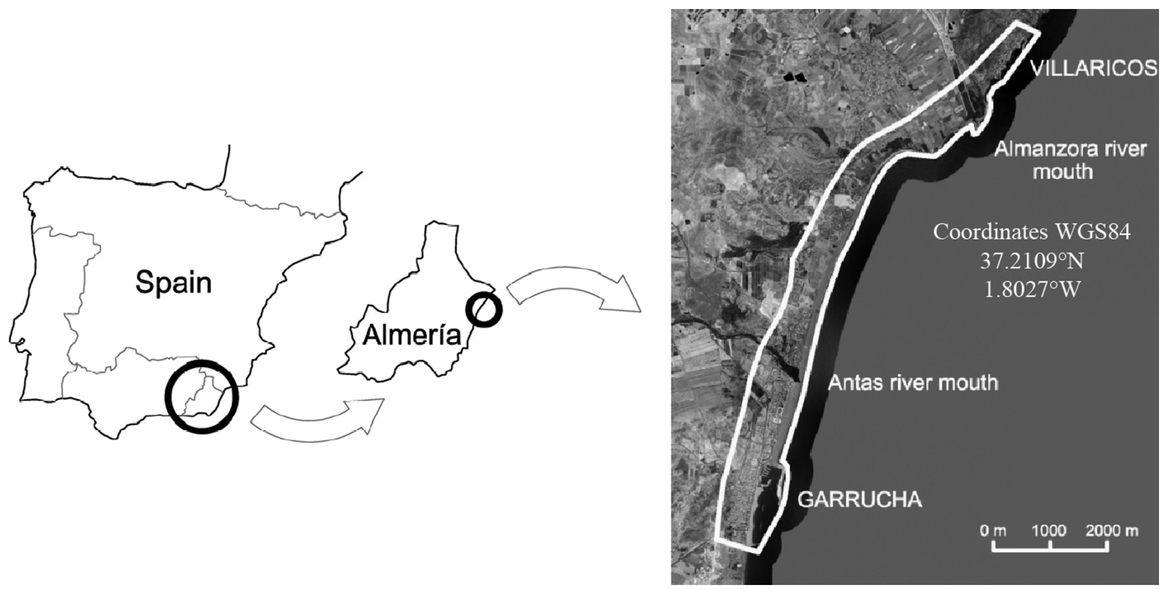

Figure 1. Location of the study site on the Almería coast, Spain.

Study Site and Data Set

Study Site

The study area comprises a heavily developed coastal fringe of Almería (Mediterranean Sea, Southern Spain), approximately 11 km long and 775 m wide. The working area is situated between the harbors of Garrucha and Villaricos (Figure 1), and is centered on the WGS84 geographic coordinates of 37.2109°N and 1.8027°W. The study area presents a smooth relief, with heights ranging from 0 m to 55 m and a mean value close to 7 m. The proliferation of touristic urbanizations along this coastal fringe during the last 50 years has provoked significant land-use and land-cover changes, likely taking part in the development of serious threats related to coastal erosion and risk of flooding.

GeoEye-1 Satellite Images

In January 2011, an image of GeoEye-1 Geo from the imagery archive of GeoEye was acquired. It was captured in reverse scan mode on 29 September 2010 recording the PAN band and all four MS bands (i.e., R, G, B, and NIR). Finally, image products were resampled to 0.5 m and 2 m for the PAN and MS cases, respectively. The clipping area extracted from the original scene was approximately occupying 49 km^2 (Figure 2), including all of the working area (850 ha). Other characteristics of the GeoEye-1 images are shown in Table 1. GeoEye-1 Geo is the GeoEye's commercial imagery format that presents the least level of corrections, both radiometric and geometric. Geo images are shipped including a sensor camera model given by the corresponding rational polynomial coefficients (RPC). Through the Geo imagery product, users can produce their own highly accurate orthorectified products by utilizing commercial off-the-shelf software and ancillary data such as DEMs and GCPs.

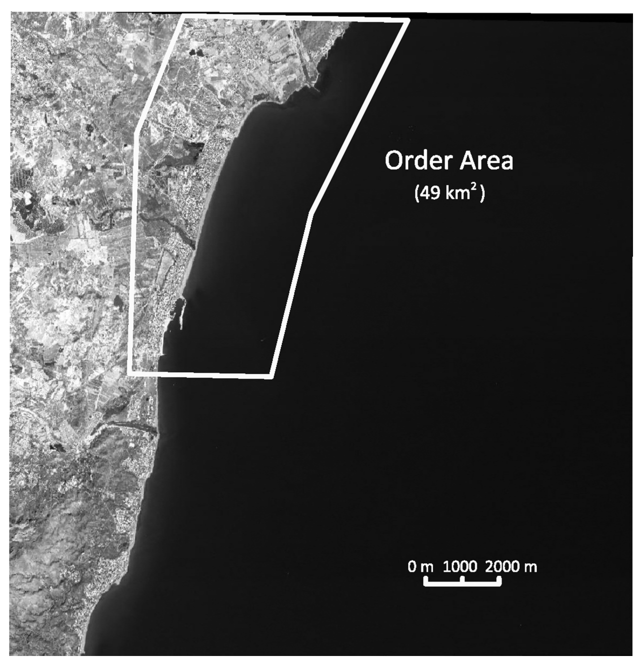

Figure 2. Order area finally acquired from the original GeoEye-1 archive scene.

Ground Control Points Collection

The ground points (GCPs and ICPs) coordinates were obtained by differential global positioning system (DGPS) using a total GPS Topcon HiPer PRO station working in real time kinematic mode (RTK). The coordinates of 119 ground points, located on well-defined features and homogeneously distributed over the study area (Figure 3) were measured with reference to the European Terrestrial Reference System 1989 (ETRS89) and UTM projection. The vertical datum took the geoid as the reference surface, adopting the mean sea level in the calm seas of Alicante (Spain) as the null orthometric height point. After adjusting the survey network, the obtained accuracies were 5.6 cm, 3.3 cm, and 7.6 cm in X, Y, and Z axes, respectively.

A high number of ground points were needed because the reliability of RMSE values depends, among other variables, on the number of ICPs used to compute them. The National Standard for Spatial Data Accuracy (NSSDA) by the

TABLE 1. CHARACTERISTICS OF THE PAN AND MS GEOEYE-1 GEO IMAGES ACQUIRED AT THE STUDY SITE

Product	GeoEye-1 Geo
Acquisition Date	29/09/10
Cloud Cover (%)	0
Source Image	2010092911015041603031603264_004
Sun Angle Azimuth	159.29 degrees
Sun Angle Elevation	48.39 degrees
Sensor Elevation Angle	69.41 degrees
Sensor Azimuth Angle	221.92 degrees
Acquired Nominal GSD Cross Scan	0.460 m PAN and 1.841 m MS
Acquired Nominal GSD Along Scan	0.449 m PAN and 1.796 m MS
Product Pixel Size	0.5 m PAN and 2 m MS

Figure 3. Distribution of 75 ICPs (black crosses) and 44 GCPs (white circles) overlaid on the GeoEye-1 panchromatic orthorectified image.

Federal Geographic Data Committee (FGDC, 1998) and the Joint Research Centre, European Commission (JRC, 2008) recommend the use of a minimum of 20 ICPs, which should be, at least, three times more accurate than the final product specification. Nevertheless, this size seems to be very small in most of cases and some authors (Li, 1991; Ariza and Atkinson, 2005; Aguilar *et al.*, 2008b) suggest larger samples.

Digital Elevation Models

In the orthorectification process of VHR satellite images it is necessary to correct the displacements due to the tilt of the sensor and to the relief of the terrain. Consequently, the participation of a DEM is fundamental. In this case, two DEMs were tested for the generation of PAN and MS orthoimages from GeoEye-1 imagery:

1. The first DEM was a medium resolution DEM with a grid spacing of 10 m. It was obtained by the Andalusia Government from a photogrammetric flight carried out during 2001 and 2002 at an approximate scale of 1:20 000. The Andalusia DEM was published in 2005 (Andalusia Government, 2005). The original DEM corresponding to the study area was transformed from UTM European Datum 1950 and orthometric heights to the new Spanish official geodetic system, i.e., ETRS89 above GRS80 ellipsoid using the minimum curvature method developed by the Spanish National Geographical Institute (González-Matesanz *et al.*, 2006). The corresponding DEM accuracy was estimated upon 62 DGPS highly accurate ICPs located at open terrain, yielding a vertical RMSE value approximately at 1.34 m.
2. The second DEM used in this work was a high accuracy and resolution lidar-derived DEM with a grid spacing of 1 m. This DEM was acquired on 28 August 2009 as a combined photogrammetric and lidar survey at a flying height above ground of approximately 1,000 m. A Leica ALS60 airborne laser scanner (35 degree field of view (FOV)) was used with the support of a nearby ground GPS reference station. The estimated vertical accuracy, in terms of RMSE, computed from 62 ICPs had a value of 8.9 cm.

Sensor Models Tested

In satellite imagery, geometric sensor models are used to relate the relationship between the three-dimensional (3D) object space positions (X, Y, Z) to their corresponding two-dimensional (2D) image space positions (x, y). For VHR satellite imagery, most of the researchers recommend the use of (a) 3D physical or rigorous models (e.g., Toutin, 2004; Wolniewicz *et al.*, 2004; Aguilar *et al.*, 2007b; Dolloff and Settergren, 2010), or (b) the well-known vendor supplied Rational Polynomial Coefficients (RPCs) refined, in image space, through a modest number of high accuracy GCPs (e.g., Grodecki and Dial, 2003; Fraser and Hanley, 2003; Tao *et al.*, 2004; Fraser and Ravanbakhsh, 2009). These two models have been tested in this work using the commercial software PCI Geomatica OrthoEngine®, version 10.3.2 (PCI Geomatics, Richmond Hill, Ontario, Canada).

3D Rational Functions with Vendor Supplied RPCs Refined with a Few GCPs

Usually, the widely used 3D rational functions are expressed in the form of two ratios of third order polynomial functions of object space coordinates. Separate rational functions are used to express the object space to line, and the object space to sample, coordinate relationships. With the physical sensor model available for commercial satellite data vendors, RPCs can be solved using an object grid with its nodes coordinates determined by means of the physical sensor model (Tao and Hu, 2001). Third order RPCs for the forward form are usually distributed by image vendor in VHR sensors such as Ikonos, QuickBird, or GeoEye-1. This method can be applied without GCPs (this is the reason why it is so-called "terrain-independent"), however the accuracy obtained is not very good. In this sense, specifications for DigitalGlobe's VHR satellites as Basic products (DigitalGlobe, 2009) without GCPs quote a systematical horizontal shift of 23 m for QuickBird, and 6.5 m for WorldView-1 and WorldView-2, all measured as Circular Error 90% (CE90). On the other hand and only using RPCs, GeoEye's VHR satellites produce accuracies in geolocation (CE90) of 15 m for Ikonos Geo and 5 m for GeoEye-1 Geo (GeoEye, 2009). In fact, orbital navigation and stability of the data have been notably improved in the newest VHR satellites. It allows them a much better automatic geolocation based only on RPCs and without GCPs.

Even so and for producing the best results, the users can update or improve the accuracy of the supplied rational function model by refining the RPCs through a few GCPs. The OrthoEngine® RPC indirect method is based on the block adjustment method developed by Grodecki and Dial (2003) for image space:

$$\Delta x = x' - x = a_0 + a_1 \cdot x + a_2 \cdot y + a_3 \cdot x \cdot y + a_4 \cdot x^2 + a_5 \cdot y^2$$

$$\Delta y = y' - y = b_0 + b_1 \cdot x + b_2 \cdot y + b_3 \cdot x \cdot y + b_4 \cdot x^2 + b_5 \cdot y^2 \quad (1)$$

where a_0 to a_5 and b_0 to b_5 are the adjustment parameters of an image, Δx and Δy express the discrepancies between the line measured and the sample coordinates for the new GCPs in the image space (x', y') and the RPCs projected coordinates for the same GCPs (x, y). For the zero order transformation (RPC0), only a simple two-dimensional shift (a_0 and b_0) is computed; because of it, only one GCP is necessary to calculate this indirect method. When an affine transformation in the image space is used (RPC1), six coefficients of the equation 1 (a_0 to a_2 and b_0 to b_2) have to be computed. Therefore it is necessary to know, at least, three GCPs. Finally, a third order 3D rational function, i.e. vendor's RPCs data refined by a second order polynomial adjustment (RPC2), is also tested in this work. In this case 12 coefficients (a_0 to a_5 and b_0 to b_5) have to be computed using, at least, six GCPs.

3D Physical Model

The rigorous, physical or parametric models are based on a standard photogrammetric approach, i.e., the collinearity equations describing the physical-geometrical image acquisition. A 3D physical model developed by Toutin (2003) at the Canada Centre for Remote Sensing (CCRS) is also tested in this work for the GeoEye-1 imagery. Even though the detailed sensor information for GeoEye-1 has not been released by the vendor, a valid solution for CCRS can be obtained using a limited number of GCPs (approximately six) and basic information from the image metafiles. Note that the image metadata supplied with GeoEye-1 Geo imagery are exactly the same that those provided by Ikonos Geo products.

Geometric Quality Assessment Tests

Orthorectification transforms the central projection of the image into an orthogonal view of the ground with uniform scale, thereby removing the distorting affects of tilt optical projection and terrain relief. The geometric error of an orthoimage can be approximated by the sum of the error due to the sensor orientation phase plus the error propagated from the uncertainty of the ancillary DEM (e.g., Aguilar *et al.*, 2006). In this work, the geopositioning capabilities of PAN and MS GeoEye-1 Geo images have been studied, both at the sensor orientation stage and at the final orthorectification phase, and always in terms of RMSE.

GeoEye-1 PAN Image Accuracy Assessment

This test has been designed to study the influence of several variables on the orthoimage geometric accuracy. During the sensor orientation phase, these variables are the sensor model (RPC0, RPC1, RPC2, and CCRS), the number of GCPs (ranging from 2 to 12) and the GCPs distribution (a qualitative variable indicating good or bad planimetric and vertical distribution). At the final orthorectification phase, the influence of the accuracy of the ancillary DEM (lidar-derived and Andalusia DEM) is also tested.

Several combinations of n GCPs (n = 2, 4, 7, 10, and 12) were generated from the 44 measured GCPs using DGPS (Figure 3). Five replicates were extracted over the study area for each number of GCPs (i.e., 25 different sets of GCPs), first looking for a good distribution, both planimetric and vertical. Another 25 new sets of GCPs were extracted from the original 44 GCPs, in this occasion assuring a bad distribution by choosing points as grouped as possible. Bearing in mind that some sensor models needed a minimum number of GCPs to be computed, only 30 projects were carried out for RPC2 and CCRS (i.e., 7, 10, and 12 GCPs sets), 40 projects for RPC1 (i.e., 4, 7, 10, and 12 GCPs sets) and, finally, 50 projects for RPC0 (i.e., using all the possible combinations of GCPs extracted). It is important to highlight that the image coordinates of each ground point remained constant for all the projects, i.e., they were only marked once in image space. On another note, all the residual populations at X and Y axes, in both sensor orientation and orthorectification phases, were tested for normality of their distribution. The Kolmogorov-Smirnov test was used as a goodness of fit to a standard normal distribution. Furthermore, no blunder errors were identified at the residual populations after applying the 3-sigma rule (Daniel and Tennant, 2001).

In order to study the influence of studied factors on the sensor orientation accuracy, an analysis of variance (ANOVA) test was carried out by means of a factorial model with five replicates (Snedecor and Cochran, 1980). In essence, ANOVA is a common statistical tool used to analyze datasets for which we are interested in evaluating the importance of several factors at once. Basically, the principles of ANOVA are the same as those for the comparison of two datasets using the well-known Student's t-test, but for which the application is extended to groups of three or more datasets. In our case, the observed variable was the planimetric RMSE ($RMSE_{2D}$), always computed at the same 75 ICPs (Figure 3). The sources of variation, or factors, were the sensor model used, the number of GCPs, the GCPs distribution over the study area, and the cross-interactions between them all. When the results of the ANOVA test turned out to be significant, the separation of means was carried out using the Duncan's multiple range test at a 95 percent confidence level.

On the other hand, ten PAN orthoimages with a GSD of 0.5 m were generated by RPC0 with the five sets of seven well-distributed GCPs, using as ancillary data both the lidar-derived DEM and Andalusia DEM. Only 48 ICPs out of the original 75 could be used for the geometric accuracy assessment at this phase, because of the pointing of some ICPs onto the orthoimages was not suitable owing to they were located at corners of buildings and as such, not being placed on the ground. A sinusoidal resampling kernel ($\sin(x)/x$ with 16×16 windows) was applied to original image cells during the orthorectification process (Toutin, 2004).

GeoEye-1 MS Image Accuracy Assessment

Owing to the GSD in the MS image of GeoEye-1 was bigger than the GSD in the PAN image, some of the ground points used at the aforementioned PAN accuracy assessment could not be employed at the MS accuracy test. In fact, only 42 GCPs and 50 ICPs (Figure 4) could be properly marked on the MS image space.

In this case, the sensor orientation accuracy was again analyzed by means of an ANOVA test. For all the residual populations, the Kolmogorov-Smirnov test was used as a goodness of fit to a standard normal distribution, and no blunders were detected. In the same way already explained along the PAN accuracy assessment, $RMSE_{2D}$, always computed at the same 50 ICPs (Figure 4), was the observed variable for the ANOVA test, using a factorial design with five repetitions. In this case, the sources of variation were the sensor model

Figure 4. Distribution of 50 ICPs (black crosses) and 42 GCPs (white circles) overlaid on the GeoEye-1 multispectral orthorectified image showed in B&W.

used (only RPC0, RPC1, and RPC2), the number of GCPs (2, 4, 7, 10, and 12, but only counting with a good distribution), and the cross-interactions between them all. When the results of the ANOVA test turned out to be significant, the separation of means was carried out using Duncan's multiple range test at a 95 percent confidence level. Summing up, and in order to carry out the geometric accuracy test on MS GeoEye-1 image, 25 projects were computed for RPC0 sensor model, 20 for RPC1, and 15 for RPC2.

Using nearly the same procedures as in the previous PAN orthoimages test, ten MS orthoimages with a GSD of 2 m were generated by RPC0 with the five sets of seven well-distributed GCPs, using as ancillary data both the lidar-derived DEM and Andalusia DEM. In this case, only 32 ICPs could be used for the geometric accuracy assessment at this phase. Again, a sinusoidal resampling kernel ($\sin(x)/x$ with 16×16 windows) was applied.

Results and Discussion

Direct Geopositioning of GeoEye-1 Products without GCPs

RPC biases, mainly attributable to small systematic errors in sensor attitude observations but also position and velocity, have a direct impact on geopositioning since the errors are translated to shifts in object space coordinates. First, for the GeoEye-1 images presented in this work, both PAN and MS, direct georeferencing projects were performed within OrthoEngine® only using the supplied RPCs and so without GCPs. Systematic errors in Easting and Northing object space coordinates of 2.65 m and 0.57 m, respectively, were registered for the PAN image on the basis of 75 permanent ICPs, whereas very similar results were attained for MS image (2.21 m and 0.67 m for Easting and Nothing coordinates, respectively) tested on 50 ICPs. These results are well inside the specified accuracy of the GeoEye-1 Geo products, i.e., 5 m CE90 or 3 m $RMSE_{2D}$. It is noteworthy that the standard deviations for the resulting two-dimensional errors in object space were of 0.33 m and 1.30 m for PAN (75 ICPs) and MS (50 ICPs) projects, respectively. These would be the best possible geopositioning accuracy results after a full bias correction, and they should be attained using only a few GCPs.

Pan-sharpened Images from Geo products of GeoEye-1

VHR satellite imagery is a valuable data acquisition tool for a variety of mapping and GIS applications such as topographic mapping, map updating, orthophoto generation, environmental monitoring, or change detection. For many of these applications, it is desirable to use pan-sharpened images (e.g., Dennison *et al.*, 2010) generated by means of image fusion of VHR PAN and MS images. For the GeoEye-1 Geo products, PAN and MS images are resampled exactly on top of each other. Therefore, it is possible to perform pan-sharpening or fusion algorithms on the original data before sensor orientation phase. In this way, the best geometric results could be obtained. Note that when a pan-sharpened image is created using the Geomatica PANSHARP algorithm, the RPC file generated for this image is exactly the same that the RPC file supplied with the PAN image. Therefore, if the marked image coordinates of GCPs and ICPs remain constant, the same geopositioning accuracy results generated for PAN image projects should also be obtained for the pan-sharpened ones. In other words, the results attained during the next step in our study for the GeoEye-1 PAN image could be directly extrapolated to the pan-sharpened image.

GeoEye-1 PAN Image Accuracy Assessment at Sensor Orientation Phase

The first statistical test was developed using the accuracy estimates ($RMSE_{2D}$), always computed at the same 75 ICPs, obtained from the 150 PAN image sensor orientation projects, being the studies factors: (a) the sensor model, (b) number of GCPs, (c) distribution of GCPs, and (d) the cross-interactions between them all. The three main factors analyzed and all their cross-interactions were significant at the 0.05 level. In fact, the qualitative factor "GCPs distribution" had the most significant repercussion in the ANOVA model (F-test around 46) followed by the "Sensor model" (F-test around 25). The cross-interaction between GCPs distribution and Sensor model was third on the list (F-test around 24). The number of GCPs and the rest of the cross-interactions presented the lowest repercussion in the ANOVA model, with F-test values around 11.

When only the 75 projects computed with well-distributed GCPs were used, i.e., excluding the qualitative variable GCPs distribution, the sensor model was the only significant factor at the 0.05 level. Only $RMSE_{2D}$ for CCRS (0.654 m) was found statistically different by applying Duncan's multiple range test for means comparison, being the worst of the sensor model tested. Thus, the other sensor models, with $RMSE_{2D}$ mean values of 0.358 m, 0.372 m, and 0.439 m for RPC0, RPC1, and RPC2, respectively, did not present statistical significant ($p < 0.05$). On the other hand, and only working with badly distributed GCPs, RPC0 was clearly the best sensor model tested. In fact, for the last model neither the distribution nor the number of GCPs had any statistic influence on the attained geopositioning accuracy.

The $RMSE_{2D}$ values generated from PAN projects at the sensor orientation phase are shown in Table 2. Note that

Table 2. Comparison of Mean Values of $RMSE_{2D}$ Computed at 75 ICPs from GeoEye-1 Panchromatic Image Depending on the Number and Distribution of GCPs; for each Sensor Model Tested, Values in the Same Column Followed by Different Superscript Letters Indicate Significant Differences at a Significance Level $p < 0.05$, i.e., for RPC0 and Good Distribution, the Value for 12 GCPs (0.340 m) is Statistically Different of Two and Four GCPs but not when seven and ten GCPs were used

Sensor Model	No. GCPs	$RMSE_{2D}$ (m) Good Distribution	$RMSE_{2D}$ (m) Bad Distribution
RPC0	2	0.375 [a]	0.385 [a]
	4	0.376 [a]	0.374 [a]
	7	0.346 [ab]	0.364 [a]
	10	0.350 [ab]	0.378 [a]
	12	0.340 [b]	0.357 [a]
RPC1	4	0.419 [a]	3.854 [a]
	7	0.353 [b]	0.937 [b]
	10	0.371 [b]	0.749 [b]
	12	0.345 [b]	0.515 [b]
RPC2	7	0.559 [a]	38.618 [a]
	10	0.375 [a]	14.246 [a]
	12	0.384 [a]	5.919 [a]
CCRS	7	1.039 [a]	152.768 [a]
	10	0.512 [a]	24.315 [b]
	12	0.410 [a]	10.759 [b]

each $RMSE_{2D}$ has been computed as the mean value of five repetitions. It is noteworthy that RPC2 and CCRS seem to be sensor models very sensitive to the number, and especially, the distribution of GCPS. RPC1 also showed a certain dependence regarding GCPs distribution, but to a much lesser extent. The best geopositioning accuracies were attained by RPC0 (regardless of the GCPs distribution) and RPC1 (only working on well-distributed GCPs), without significant differences between them.

With regard to the number of GCPs used for RPC0, and looking at Table 2, although this factor were not significant when poorly-distributed GCPs were used, slightly better accuracies were computed for well-distributed GCPs when the number of GCPs was of seven or more. In the same way, for RPC1, at least seven well-distributed GCPs were needed to obtain the best sensor orientation results. Summing up, the best accuracies using RPC0 or RPC1 with seven GCPs were to around 0.35 m, being very similar to the aforementioned best possible geopositioning accuracies of 0.33 m. Moreover, Fraser and Hanley (2005) pointed out the shift-only bias correction (RPC0) as the best sensor model for the reverse scanned Ikonos Geo stereo imagery, mainly due to its steady scanning mode. On the other hand, and regarding VHR satellite images with higher order error sources such as perturbations in scan velocity (e.g., Ikonos forward scanned images and QuickBird imagery), shift and drift model, full affine correction model (i.e., RPC1) or RPC2 could attain better results (e.g., Fraser and Hanley, 2005; Aguilar *et al.* 2008a; Tong *et al.*, 2010). The differences between RPC0 and RPC1 results will be analyzed more in depth in the next section.

Very similar results were reported by Meguro and Fraser (2010) using a stereopair of pan-sharpened GeoEye-1 images. In fact, they applied the RPC0 model to obtain a two-dimensional geopositioning accuracy, measured at 115 ICPs, of 0.38 m (almost the same result as in our work). Other authors, working on very varied Ikonos imagery (along-track and cross-track stereopairs, stereo triplets, single images) and using RPC-bias correction, achieved $RMSE_{2D}$ ranging from 1.59 to 0.73 m (Fraser and Hanley, 2005; Li *et al.*, 2009; Xiong and Zhang, 2009). Furthermore, a lot of similarities can be drawn between the present paper and a previously published work by Aguilar *et al.* (2008a) where a single Ikonos Geo image was tested. In this case, the $RMSE_{2D}$ estimated for Ikonos turned out to be of 0.60 m, 0.63 m, and 1.09 m by using RPC0, RPC1, and CCRS sensor models, respectively (these same values could be expressed in pixels bearing in mind that Ikonos PAN imagery presents a GSD of 1 m). On the other hand, for GeoEye-1 PAN imagery presenting a GSD of 0.5 m, and analyzing all of the repetitions generated with well-distributed GCPs in this work, the normalized $RMSE_{2D}$ would range from 0.67 to 0.84 pixels (mean value of 0.72 pixels) for RPC0, from 0.65 to 0.94 pixels (mean value of 0.74 pixels) for RPC1, and, finally, from 0.74 to 5.58 pixels (mean value of 1.31 pixels) for CCRS sensor model. In summary, although GeoEye-1 direct geopositioning without GCPs has been clearly improved in relation to Ikonos, the bias-free geopositioning accuracy expressed in pixels of the newest GeoEye's VHR satellite may be considered as very similar to the most ancient VHR satellite. On another note, Fraser and Ravanbakhsh (2009) achieved vertical and horizontal accuracies of 0.50 and 0.25 pixels, respectively, using a stereopair of GeoEye-1 supported by extremely accurate measured ground points, both in object and image space. Therefore, the best geopositioning accuracy around to 0.7 pixels, attained under operational conditions, might be still improved.

With regard to CCRS model, and as it is widely known, each independently acquired line of the pushbroom scanner imagery has its own time-dependent attitude angles and perspective center position. In fact, that detailed sensor and satellite information is released by DigitalGlobe but not by GeoEye. It is why some authors (e.g., Tao *et al.*, 2004) pointed out the difficulty to develop a parametric sensor model that reflects the physical reality of the complete viewing geometry for the Ikonos sensor. The same could be said in the case of GeoEye-1. In this way, very poor results have been attained in this work using the CCRS physical model embedded within OrthoEngine®. In addition, quite poor sensor orientation accuracies of around 1 to 2 pixels in horizontal components were also reported by Crespi *et al.* (2010) working with a PAN GeoEye-1 stereopair and using the CCRS model.

RPC0 versus RPC1

At this point, a further comparison between the best two sensor models for correcting bias from GeoEye-1 Geo PAN images is carried out. Until now, only global horizontal accuracy has been studied, concluding that both RPC0 (almost regardless of the number and distribution of the GCPs used) and RPC1 (with at least seven well-distributed GCPs) would be the best choice. But systematic errors or bias could be registered along X and Y axes. In this way, the mean values of the residuals for X and Y axes were computed on the 75 ICPs using the sensor orientation given by the RPC0 and RPC1 sensor models with the support of seven well-distributed GCPs. Note that there were five repetitions for each sensor model tested. The original systematic errors of RPCs in object space coordinates of 2.65 m in Easting and 0.57 m in Northing, previously reported for the PAN image, were effectively removed using both RPC0 and RPC1, although RPC1 depicted slightly better results (Table 3). Moreover, both of sensor models tended to work better in the cross-track than in the along-track direction, which might be indicating disturbances in the sensor scan velocity. On another note, full affine correction model (RPC1) achieved to slightly correct that along-track bias. In Table 3, the upper and lower limits for the computed mean value at 95 percent confidence level are also shown. These limits can be estimated as follows:

$$Limits = Mean \pm \frac{1.96 \times \sigma_{\text{mean}}}{\sqrt{75}} \quad (2)$$

where *Mean* represents the mean value of the residuals calculated at the 75 ICPs, and σ_{mean} is the standard deviation for each repetition.

TABLE 3. MEAN VALUES OF THE RESIDUALS FOR X AND Y AXES AND THEIR CORRESPONDING UPPER AND LOWER LIMITS AT 95 PERCENT CONFIDENCE LEVEL; THE RESIDUALS WERE COMPUTED AT 75 ICPS DURING THE SENSOR ORIENTATION PHASE FOR THE PANCHROMATIC IMAGE; THE MEAN VALUES IN BOLD REPRESENT THE CASES IN WHICH THE ZERO VALUE FELL OUT OF THE COMPUTED LIMITS

		RPC0 with 7 GCPs well distributed			RPC1 with 7 GCPs well distributed		
Repetition	Axis	Mean (m)	Lower Limit	Upper Limit	Mean (m)	Lower Limit	Upper Limit
1	X	–0.009	–0.056	0.038	–0.026	–0.073	0.021
	Y	0.001	–0.057	0.059	0.030	–0.028	0.088
2	X	0.017	–0.030	0.064	–0.019	–0.070	0.031
	Y	**–0.059**	–0.116	–0.001	–0.051	–0.107	0.004
3	X	**0.094**	0.047	0.141	0.028	–0.032	0.087
	Y	**–0.183**	–0.241	–0.125	**–0.105**	–0.169	–0.040
4	X	0.041	–0.006	0.088	–0.004	–0.056	0.048
	Y	**–0.069**	–0.127	–0.011	–0.040	–0.094	0.015
5	X	0.015	–0.033	0.062	–0.006	–0.064	0.052
	Y	**–0.103**	–0.160	–0.045	**–0.089**	–0.145	–0.033

In the absence of systematic errors, the mean of residuals should be close to zero, but, as can be seen in Table 3, there are some cases where the mean value are not included within the computed limits. For RPC0, five out of the ten cases fell out of the confidence interval, whereas only two cases presented possible systematic errors for RPC1.

The plots of ground coordinate residuals shown in Figure 5 provide another point of view. In that figure, the best repetition (number 1 in Table 3) and the worst (number 3 in Table 3) were analyzed for RPC0 and RPC1. For the residuals coming from repetition 1, Figures 5a and 5b show a quite random distribution suggesting the absence of any further systematic error. Nonetheless, for repetition 3 and RPC0 sensor model (Figure 5c), the northern residuals present a little bias towards south-east, probably caused by some GCPs not very well positioned on the image. Those biases could be reduced by RPC1 sensor model.

Taking into account that RPC1 has turned out to be sensitive to both the number and location of GCPs, and given that the removal of systematic errors respect to RPC0 has not been excessively significant, it seems reasonable to recommend the RPC0 sensor model for the sensor orientation phase of GeoEye-1 PAN images, as it has been already reported by Fraser and Ravanbakhsh (2009) and Meguro and Fraser (2010).

GeoEye-1 MS Image Accuracy Assessment at Sensor Orientation Phase

A huge amount of research has been focused on the geopositioning assessment of PAN or pan-sharpened VHR satellite imagery from different sensors both using RPCs refined with a few GCPs and rigorous 3D physical models. However, scientific researches involving the use of MS VHR satellite imagery have been, until now, mainly addressed to identify a broader range of land features (i.e., image classification). Bearing in mind that features extracted by image classification have to be based on proper georeferencing (e.g., high accuracy MS orthoimages), a number of studies about MS images geopositioning accuracy are necessary. In other words, because classification accuracy depends on geometric accuracy, we have to search for the potential geopositioning accuracy offered by VHR satellites MS imagery under operational conditions.

In this case, the ANOVA test was carried out on the $RMSE_{2D}$ (observed variable computed at 50 ICPs) along a total of 60 MS image sensor orientation projects. The studied factors were the followings: (a) the sensor model, (b) the number of GCPs, and (c) the cross-interactions between them all. Of all of them, only the sensor model was significant at the $p < 0.05$ level. Solely, $RMSE_{2D}$ for RPC2 (1.535 m) was found statistically different of RPC0 one (1.385 m) applying Duncan's multiple range test for means comparison. Nevertheless, no significant differences were observed either between RPC0 and RPC1 (1.449 m) or RPC1 and RPC2.

The geopositioning accuracy results for the MS Geo-Eye-1 image are depicted in Table 4. It is relevant to notice that the number of GCPs only had some statistical influence on the obtained $RMSE_{2D}$ in the RPC0 case. It seems that only two GCPs were not enough for achieving the best results. Nevertheless, when seven evenly-distributed GCPs were used, fairly concentrated $RMSE_{2D}$ values ranging from 1.366 m (0.68 pixels) to 1.308 m (0.65 pixels) were attained. These geopositioning accuracies turned out to be very similar to the standard deviation of 1.30 m previously calculated for the MS project using RPCs without GCPs. Furthermore, the best accuracies achieved in this work during the sensor orientation phase, both using PAN and MS images, coincide with those reported by Meguro and Fraser (2010) using pan-sharpened GeoEye-1 images, i.e., all of them being close to 0.7 pixels. Moreover, based on nearly a decade of experience with VHR satellites, Fraser and Ravanbakhsh (2009) inferred that geopositioning accuracy to around 0.5 to 0.7 pixels in planimetry would be readily achievable from the GeoEye-1 imagery by using refined RPCs with a few high accuracy GCPs.

Accuracy Assessment of GeoEye-1 PAN Orthoimages

Table 5 shows the errors at the ICPs generated from PAN orthorectified GeoEye-1 images using the two different DEMs described along the corresponding section. Five orthorectification projects were performed for each one of the repetitions or sets of seven well-distributed GCPs, always using RPC0 sensor model. Geopositioning accuracies during the initial sensor orientation phase are also depicted in Table 5.

The error produced in the orthoimage would be the result of the sum of the error corresponding to the sensor orientation plus the one propagated by the DEM through the orthorectification process. Thus RMSE in X, Y and two-dimensional error attained at the two different phases should present a clear relationship. When a very accurate lidar-derived DEM was used for the orthorectification process, increases ranging from 0.09 m to 0.14 m were transferred to the $RMSE_{2D}$ achieved in the orientation stage. Nevertheless, when a DEM with an estimated vertical accuracy of 1.34 m was used (Andalusia DEM), the increases rose up to values of between 0.26 m and 0.30 m. In this way, the vertical accuracy of the ancillary DEM has demonstrated to be significant for the final orthoimage geopositioning accuracy. On the other hand, almost any difference is shown in Table 5 between RMSE in X and Y axes for the orthoimages accuracy assessment. In the same way, Figure 6 only depicts random errors but not systematic errors.

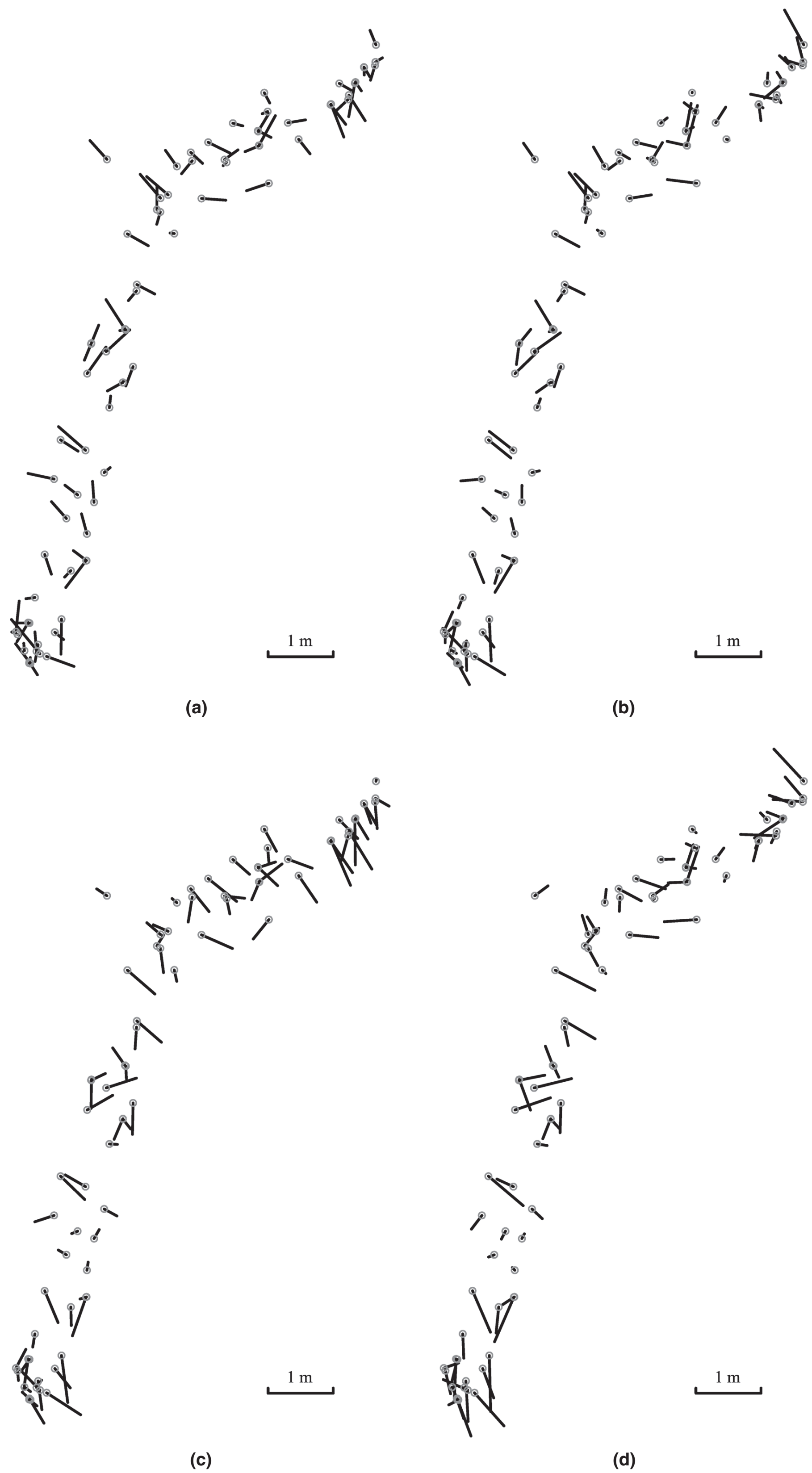

Figure 5. Ground coordinate residuals distribution from panchromatic image after orientation phase in 75 ICPs for seven well-distributed GCPs: (a) First repetition for RPC0 sensor model, (b) First repetition for RPC1 sensor model, (c) Third repetition for RPC0 sensor model, and (d) Third repetition for RPC1 sensor model.

Table 4. Comparison of Mean Values of $RMSE_{2D}$ Computed at 50 ICPs from GeoEye-1 Multispectral Image Depending on the Number of GCPs; for Each Sensor Model Tested, Values in the Same Column Followed by Different Superscript Letters Indicate Significant Differences at a Significance Level $p < 0.05$, i.e., for RPC0, the Value for Two GCPs (1.494 m) is Statistically Different of the other Values Attained for RPC0 and 4, 7, 10, and 12 GCPs.

Sensor Model	No. GCPs	$RMSE_{2D}$ (m) Good Distribution
RPC0	2	1.494 [a]
	4	1.394 [b]
	7	1.331 [b]
	10	1.362 [b]
	12	1.330 [b]
RPC1	4	1.484 [a]
	7	1.581 [a]
	10	1.379 [a]
	12	1.351 [a]
RPC2	7	1.663 [a]
	10	1.440 [a]
	12	1.502 [a]

Moreover, in the final orthoimages, RMSE errors in X or Y axes to around 0.33 m were reported using the lidar-derived DEM while these errors were increased around to 0.44 m when Andalusia DEM was utilized. Both geopositioning accuracies could be deemed as superb, taking into account that the maximum RMSE errors in X or Y directions recommended by ASPRS Interim Accuracy Standards for Large Scale Maps (ASPRS, 1989) are 0.25 m and 0.5 m for 1:1000 and 1:2000 scale Class 1 product, respectively. In addition to this, the $RMSE_{2D}$ computed on the orthoimages produced from the lidar-derived DEM was ranging from 0.432 m to 0.480 m. These are very outstanding results because, in fact, it is unusual to find research work achieving sub-pixel horizontal accuracies for PAN VHR satellite orthoimages.

VHR satellite sensors have a very narrow FOV, so that in principle, the effect of the DEM error on the produced orthoimages could be reduced almost to zero if images are collected as close to nadir as possible. However, in practice the sensors can rotate (which implies more flexibility and revisit capabilities) and most of the space imagery is collected with off-nadir angle. It is noteworthy that our GeoEye-1 image presented an off-nadir angle of more than 20°. Because of this fact, it is not the ideal product for obtaining the most accurate orthorectification process. On another note, the two tested DEMs have a very good vertical accuracy and that might reduce the propagated error due to the high off-nadir angle of the GeoEye-1 image used in this work. In this way, the fact that the study area was very small and the relief very smooth undoubtedly influenced on computing these very good orthoimage geopositioning accuracies.

Accuracy Assessment of GeoEye-1 MS Orthoimages

Table 6 shows the estimated geopositioning accuracies of the MS orthoimages. Again, the RPC0 sensor model, five repetitions of seven well-distributed GCPs, and two DEMs were used for the orthoimages generation. Unlike the PAN images, slight along-track biases were detected for MS images, in both orientation and orthorectification phases.

However, as in PAN images case, a very good sub-pixel geopositioning accuracy of 0.781 pixels and 0.805 pixels were calculated in the MS orthoimages using lidar-derived and photogrammetric DEMs, respectively. In MS satellite images, with such a bigger GSD, the vertical accuracy of the ancillary DEM used for the orthorectification process played a less important role in the final orthoimage geometric accuracy. Thus, working with MS GeoEye-1 images, it is not necessary to count on a DEM as accurate as our lidar-derived DEM to obtain a sub-pixel geopositioning accuracy. In fact, the lidar-derived DEM added a mean $RMSE_{2D}$ of 0.231 m over the $RMSE_{2D}$ obtained in the orientation phase, whereas the Andalusia DEM increased the orientation phase two-dimensional uncertainty around to 0.279 m. Moreover, and through the different repetitions carried out, it can be observed that these increases were very changeable, presenting standard deviations of 0.164 m and 0.107 m for lidar-derived and photogrammetric DEMs, respectively. It is noteworthy that these standard deviations corresponding to the PAN images ranged from 0.025 m to 0.015 m for lidar-derived and Andalusia DEMs, respectively. Undoubtedly, starting from a GSD of 2 m for MS GeoEye-1 images, it is cumbersome to identify and mark the ground points in the image space, which provokes a clearly higher image pointing error than in the case of PAN images.

Conclusions

Based on the exhaustive and rigorous statistical analysis carried out along this work, the following conclusions can be soundly drawn:

- Under operational conditions, RPC0 sensor model attained the best geopositioning accuracy during the orientation phase for both PAN and MS GeoEye-1 images. Moreover, its behavior turned out to be practically independent of the number and distribution of the GCPs used. However, and although RPC0 mathematical model could be computed only using one GCP, more than four GCPs would be recommended for a better compensation of the pointing error in image space. In this way, sub-pixel geopositioning accuracies around to 0.70 pixels might be attained for both PAN and MS GeoEye-1 images.
- With regard to PAN images, it might be worth testing RPC1 sensor model in order to reduce potential systematic errors, although at least seven well-distributed and high accurate GCPs would be needed. Anyway, the expected horizontal

Table 5. RMSE Values along X and Y Axes, and Two-dimensional Error Measured after Applying the Computed Sensor Orientation (75 ICPs) and Over the Orthorectified Imagery (48 ICPs) from GeoEye-1 Panchromatic Image; for Each Repetition, Values Were Computed Using the RPC0 Sensor Model and Seven Evenly-distributed GCPs

Repetition	Sensor Orientation Phase ICPs RMSE (m)			Orthoimage (Lidar DEM) ICPs RMSE (m)			Orthoimage (Andalusia DEM) ICPs RMSE (m)		
	X	Y	2D	X	Y	2D	X	Y	2D
1	0.207	0.254	0.328	0.325	0.319	0.456	0.396	0.458	0.605
2	0.208	0.260	0.333	0.295	0.315	0.432	0.418	0.469	0.628
3	0.227	0.313	0.387	0.339	0.330	0.473	0.471	0.440	0.644
4	0.211	0.263	0.337	0.343	0.337	0.480	0.448	0.431	0.622
5	0.207	0.274	0.343	0.350	0.329	0.480	0.444	0.417	0.609
Mean	0.212	0.273	0.346	0.330	0.326	0.464	0.435	0.443	0.622

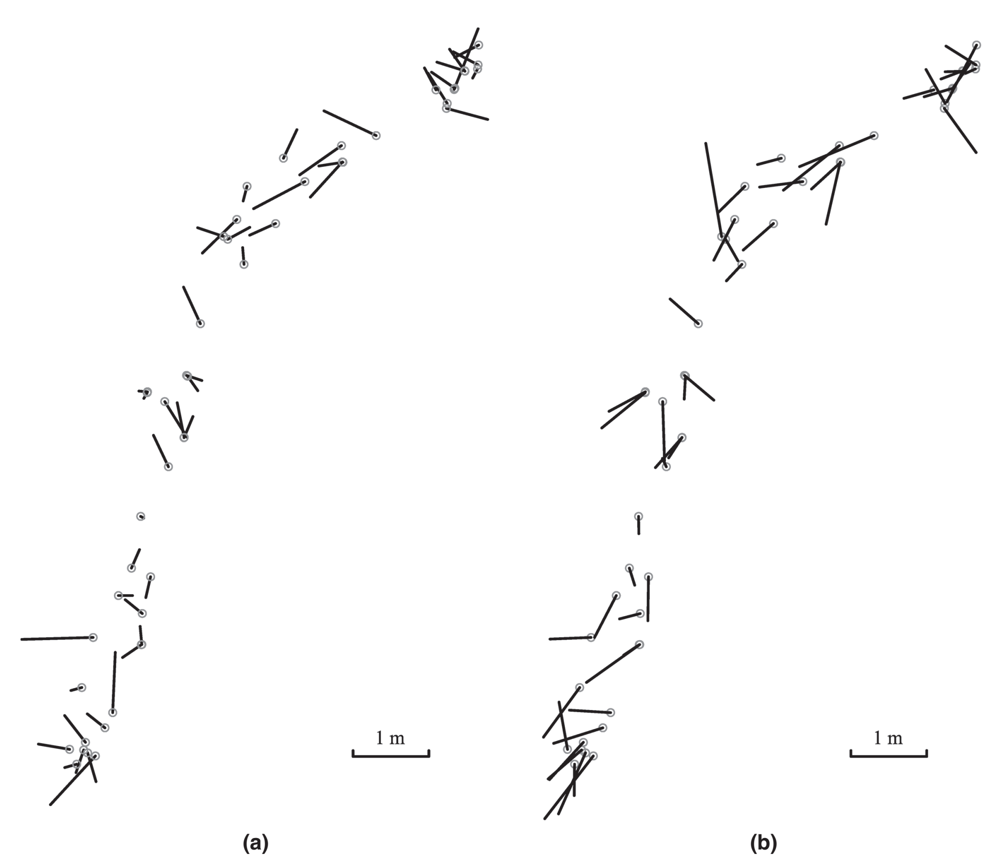

Figure 6. Ground coordinate residuals distribution in 48 ICPs for panchromatic orthorectified images derived from the first repetition for RPC0 sensor model using seven well-distributed GCPs: (a) Orthorectification process using the lidar-derived DEM, and (b) Orthorectification process using the Andalusia DEM.

TABLE 6. RMSE VALUES ALONG X AND Y AXES, AND TWO-DIMENSIONAL ERROR MEASURED AFTER APPLYING THE COMPUTED SENSOR ORIENTATION (50 ICPS) AND OVER THE ORTHORECTIFIED IMAGERY (32 ICPS) FROM GEOEYE-1 MULTISPECTRAL IMAGE; FOR EACH REPETITION, VALUES WERE COMPUTED USING THE RPC0 SENSOR MODEL AND SEVEN EVENLY-DISTRIBUTED GCPS

Repetition	Sensor Orientation Phase ICPs RMSE (m)			Orthoimage (Lidar DEM) ICPs RMSE (m)			Orthoimage (Andalusia DEM) ICPs RMSE (m)		
	X	Y	2D	X	Y	2D	X	Y	2D
1	0.846	1.009	1.317	0.810	1.197	1.445	0.903	1.214	1.513
2	0.805	1.031	1.308	0.973	1.387	1.694	0.920	1.485	1.747
3	0.911	1.018	1.366	0.811	1.212	1.458	0.907	1.284	1.572
4	0.891	1.014	1.350	0.806	1.223	1.464	0.896	1.281	1.563
5	0.817	1.029	1.314	0.918	1.485	1.746	0.947	1.358	1.655
Mean	0.854	1.020	1.331	0.863	1.301	1.562	0.915	1.324	1.610

accuracies would be very similar to those achieved with RPC0 sensor model.

- For producing orthoimages from PAN GeoEye-1 images seeking for sub-pixel horizontal accuracy ($RMSE_{2D}$ <0.5 m), it was necessary to use a very accurate lidar-derived DEM with a $RMSE_z$ around to 0.09 m. Nevertheless, using a photogrammetrically-derived DEM with an estimated $RMSE_z$ close to 1.34 m, sub-pixel geopositioning accuracies around to 1.610 m could be attained from MS GeoEye-1 images. These impressive geopositioning accuracies, together with the very short revisit time, turn these products in a very useful tool for many scientific and technical fields.
- It is noteworthy that the presented results have been achieved on a single and clipped image of GeoEye-1 over a particular working area. Thus, further works in other field conditions would be advisable to test the geopositioning accuracy capabilities of GeoEye-1 images.

Acknowledgments

This work was supported by the Spanish Ministry for Science and Innovation (Spanish Government) and the European Union (FEDER funds) under Grant Reference CTM2010-16573. The authors also appreciate the support from Andalusia Regional Government, Spain through the Excellence Research Project RNM-3575.

References

Aguilar, F.J., M.A. Aguilar, F. Carvajal, and F. Agüera, 2006. An integrated model to estimate the accuracy of digital orthoimages from high resolution satellite imagery, *Revue Française de Photogrammétrie et de Télédétection*, 184:11–16.

Aguilar, F.J., F. Carvajal, M.A. Aguilar, and F. Agüera, 2007a. Developing digital cartography in rural planning applications, *Computers and Electronics in Agriculture*, 55(2):89–106.

Aguilar, M.A., F.J. Aguilar, F. Agüera, and J.A. Sánchez, 2007b. Geometric accuracy assessment of QuickBird basic imagery using different operational approaches, *Photogrammetric Engineering & Remote Sensing*, 73(12):1321–1332.

Aguilar, M.A., F. Agüera, F.J. Aguilar, and F. Carvajal, 2008a. Geometric accuracy assessment of the orthorectification process from very high resolution satellite imagery for Common Agricultural Policy purposes, *International Journal of Remote Sensing*, 29(24):7181–7197.

Aguilar, M.A., F.J. Aguilar, and F. Agüera, 2008b. Assessing geometric reliability of corrected images from very high resolution satellites, *Photogrammetric Engineering & Remote Sensing*, 74(12):1551–1560.

Andalusia Government, 2005. *Modelo Digital del Terreno de Andalucía, Relieve y orografía*, Junta de Andalucía, Sevilla, Spain (on DVD).

Ariza, F.J., and A.D.J. Atkinson, 2005. Sample size and confidence when applying the NSSDA, *Proceedings of the 21th International Cartographic Conference*, 09-16 July, A Coruña, Spain (The International Cartographic Association), unpaginated CD-ROM.

ASPRS, 1989. ASPRS interim accuracy standards for large scale maps, *Photogrammetric Engineering & Remote Sensing*, 56(10):1038–1040.

Crespi, M., P. Capaldo, F. Fratarcangeli, A. Nascetti, and F. Pieralice, 2010. DSM generation from very high optical and radar sensors: Problems and potentialities along the road from the 3D geometric modeling to the surface model, *Proceedings of the 30th IEEE International Geoscience and Remote Sensing Symposium, IGARSS* 2010, 25-30 July, Honolulu, pp. 3596–3599.

Daniel, C., and K. Tennant, 2001. DEM quality assessment, *Digital Elevation Model Technologies and Applications: The DEM Users Manual* (D.F. Maune, editor), American Society for Photogrammetry & Remote Sensing, Bethesda, Maryland, pp. 395–440.

Dennison, P.E., A.R. Brunelle, and V.A. Carter, 2010. Assessing canopy mortality during a mountain pine beetle outbreak using GeoEye-1 high spatial resolution satellite data, *Remote Sensing of Environment,* 114(2010):2431–2435.

DigitalGlobe, Inc., 2009. DigitalGlobe Basic Imagery, URL: *http://www.digitalglobe.com/products#imagery&basic-satellite-imagery* (last date accessed: 05 December 2011).

Dolloff, J., and R. Settergren, 2010. An assessment of WorldView-1 positional accuracy based on fifty contiguous stereo pairs of imagery, *Photogrammetric Engineering & Remote Sensing*, 76(8):935–943.

FGDC, 1998. Geospatial Positioning Accuracy Standards Part 3: National Standard for Spatial Data Accuracy, URL: *http://www.fgdc.gov/standards/projects/FGDC-standards- projects/accuracy/part3/chapter3*, U.S. Federal Geographic Data Committee, Reston, Virginia (last date accessed: 05 December 2011).

Fraser, C.S., and H.B. Hanley, 2003. Bias compensation in rational function for Ikonos satellite Imagery, *Photogrammetric Engineering & Remote Sensing*, 69(1):53–57.

Fraser, C.S., and H.B. Hanley, 2005. Bias-compensated RPCs for sensor orientation of high-resolution satellite imagery, *Photogrammetric Engineering & Remote Sensing*, 71(8):909–915.

Fraser, C.S., and M. Ravanbakhsh, 2009. Georeferencing accuracy of GeoEye-1 imagery, *Photogrammetric Engineering & Remote Sensing*, 75(6):634–638.

GeoEye, Inc., 2009. GeoEye Product Guide, URL: *http://www.geoeye.com/CorpSite/assets/docs/brochures/GeoEye_Product_Guide.pdf* (last date accessed: 05 December 2011).

González-Matesanz, J., J.A. Malpica., and A. Dalda, 2006. A range of ED50-ETRS89 datum transformation models tested on the Spanish Geodetic Network, *Survey Review*, 38(102):654–667.

Grodecki, J., and G. Dial, 2003. Block adjustment of high-resolution satellite images described by rational polynomials, *Photogrammetric Engineering & Remote Sensing*, 69(1):59–68.

JRC, Joint Research Centre, ISPRA, 2008. Guidelines for Best Practice and Quality Checking of Ortho Imagery, ver. 3.0, URL: *http://www.marine.ie/NR/rdonlyres/57770D8F-9854-4012-B3CD-B2ADEB7551DA/0/OrthoImageryGuidelinesITT1132.pdf* (last date accessed: 05 December 2011).

Kay, S., P. Spruyt, and K. Alexandrou, 2003. Geometric quality assessment of orthorectified VHR space image data, *Photogrammetric Engineering & Remote Sensing*, 69(5):484–491.

Li, Z., 1991. Effects of check points on the reliability of DTM accuracy estimates obtained from experimental tests, *Photogrammetric Engineering & Remote Sensing*, 57(10):1333–1340.

Li, R., F. Zhou, X. Niu, and K. Di, 2007. Integration of Ikonos and QuickBird imagery for geopositioning accuracy analysis, *Photogrammetric Engineering & Remote Sensing*, 73(9):1067–1074.

Li, R., X. Niu, C. Liu, B. Wu, and S. Deshpande, 2009. Impact of imaging geometry on 3D geopositioning accuracy of stereo Ikonos imagery, *Photogrammetric Engineering & Remote Sensing*, 75(9):1119–1125.

Liu, J., R. Li, S. Deshpande, X. Niu, and T. Shih, 2009. Estimation of blufflines using topographic lidar data and orthoimages, *Photogrammetric Engineering & Remote Sensing*, 75(1):69–79.

Mitchell, G., and K. MacNabb, 2010. High resolution stereo satellite elevation mapping accuracy assessment, *Proceedings of the 2010 Annual ASPRS Conference*, 26–30 April, San Diego, California, unpaginated CD-ROM.

Meguro, Y., and C.S Fraser, 2010. Georeferencing accuracy of GeoEye-1 stereo imagery: Experiences in a Japanese test field, *International Archives of the Photogrammetry, Remote Sensing and Spatial Information Science*, Volume XXXVIII, Part 8, ISPRS Commission VIII, pp. 1069–1072.

Muslim, A.M., and G.M. Foody, 2008. DEM and bathymetry estimation for mapping a tide-coordinated shoreline from fine spatial resolution satellite sensor imagery, *International Journal of Remote Sensing*, 29(15):4515–4536.

Snedecor, G.W., and W.G. Cochran, 1980, *Statistical Methods*, Seventh edition, Iowa State University Press, Ames, Iowa, 507 pages.

Tao, C.V., and Y. Hu, 2001. A comprehensive study of the rational function model for photogrammetric processing, *Photogrammetric Engineering & Remote Sensing*, 67(12):1347–1357.

Tao, C.V., Y. Hu, and W. Jiang, 2004. Photogrammetric exploitation of IKONOS imagery for mapping applications, *International Journal of Remote Sensing*, 25(14):2833–2853.

Tong, X., S. Liu, and Q. Weng, 2010. Bias-corrected rational polynomial coefficients for high accuracy geo-positioning of QuickBird stereo imagery, *ISPRS Journal of Photogrammetry and Remote Sensing*, 65(2010):218–226.

Toutin, T., 2003. Error tracking in Ikonos geometric processing using a 3D parametric model, *Photogrammetric Engineering & Remote Sensing*, 69(1):43–51.

Toutin, T., 2004. Review article: Geometric processing of remote sensing images: models, algorithms and methods, *International Journal of Remote Sensing*, 25(10):1893–1924.

Wolniewicz, W., 2004. Assessment geometric accuracy of VHR satellite images, *Proceeding of the XXth International Archives of the Photogrammetry, Remote Sensing and Spatial Information Sciences*, 12-23 July, Istanbul, Turkey, 35(Part B1), unpaginated CD-ROM.

Xiong, Z., and Y. Zhang, 2009. A generic method for RPC refinement using ground control information, *Photogrammetric Engineering & Remote Sensing*, 75(9):1083–1092.

(Received 24 May 2011; accepted 05 September 2011; final version 12 September 2011)